Assessing the Orbiter Thermal Environment Using Flight Data

S.D. Williams*
Lockheed Engineering and Management Services Company, Inc., Houston, Texas

and

Donald M. Curry†
NASA Lyndon B. Johnson Space Center, Houston, Texas

A unified analysis of the Shuttle Orbiter aerothermodynamic environment and thermal protection system performance is presented using the Space Transportation System development flight data. Comparisons of predicted and measured temperatures and heating rates along the Orbiter lower windward fuselage centerline and lower wing 50% and 80% semispans are discussed. The results of this study indicate lower than predicted heating on windward fuselage surface, but higher heating on the nose cap and 50% semispan wing panels.

Nomenclature

C_p = specific heat at constant pressure
H_T = total enthalpy
h = film heat transfer coefficient
h_{ref} = reference film heat transfer coefficient
K = thermal conductivity
$\dot{q}_{conv}$ = convective heating rate
$\dot{q}_{net}$ = net heating rate
$\dot{q}_{ref}$ = reference heating rate
Re = Reynolds number
Re_∞ = freestream Reynolds number
Re_{NS} = normal shock Reynolds number
T = temperature
T_{sink} = sink temperature
T_{surf} = surface temperature
α = angle of attack
Δt = time step size
Δx = space step size
ϵ = emittance or emissivity
σ = Stefan-Boltzmann constant
ρ = density

Introduction

THE key to the development of a multimission, low-cost, weight-effective Orbiter thermal protection system (TPS) was the selection of unique reusable materials which could withstand the high-temperature environment and/or system design which could provide adequate insulation for the structure and internal systems. The Orbiter TPS consists of four different material configurations: coated reinforced carbon-carbon (RCC) for nose and wing leading edge areas where entry temperatures exceed 2300° F, high-temperature reusable surface insulation (HRSI) for temperatures between 1200 and 2300° F, low-temperature reusable surface insulation (LRSI) between 700 and 1200° F, and flexible reusable surface insulation (FRSI) for areas with surface temperatures not exceeding 700° F. Therefore, the ability to predict the Orbiter thermal environment accurately was of utmost importance in the TPS design.

During the design phase of the Shuttle Orbiter, the primary analysis was concerned with the thermal performance of the competing TPS configurations. Usually this assessment was directed toward minimizing TPS weight while maintaining design structural temperature limitations.[1] Also of importance was the need to assess the thermal conductivity of TPS candidates rapidly in order not only to verify the thermophysical properties but also to evaluate the property variation in prototype specimens.[2] A natural extension of this analysis capability was to determine the surface conditions (temperature and heating rate) from a single embedded thermocouple.[3] This permits the complete assessment of a material from ground test data through the evaluation of the performance of the TPS using flight data.

Measurements of surface and in-depth thermocouple temperatures on the TPS for the initial five Orbiter flights have provided sufficient data to assess the aerothermal environment in terms of predicted and measured temperatures and surface heating rates. The methodology used in defining the Orbiter design heating environment consisted of a nominal trajectory for the most severe operation mission, state-of-the-art flow models (i.e., flat plate, sphere, cone, wedge), normalized to nominal wind tunnel (W.T.) heat transfer data to obtain flight heating predictions, nominal material properties, and aerodynamically smooth surfaces.[4] Comparisons of flight- and wind tunnel-derived heating provide a basis for improvements in the current analytical techniques used to predict the aerothermodynamic environment to the Orbiter vehicle. Detailed comparisons of selected flight data and vehicle locations with various theoretical aerothermodynamic heating techniques (i.e., chemical equilibrium, nonequilibrium flow, material finite catalycity, etc.) are available.[5]

This paper presents the results of a unified thermal analysis, i.e., temperature/heat flux predictions, performed at selected locations on the Shuttle Orbiter windward surface to assess the nominally predicted aerothermodynamic environment and TPS response characteristics with the Space Transportation System (STS) flight data. Results are presented for the RCC nose cap (NC) and wing leading edge (WLE), Orbiter lower fuselage centerline, and the lower wing surface 50% and 80% semispans. The analyses are presented in terms of surface temperature and heating rate time histories, in-depth material thermal response, percent errors in radiation equilibrium heating rates, heating rates as a function of location on the vehicle,

Presented as Paper 83-1488 at the AIAA 18th Thermophysics Conference, Montreal, Canada, June 1-3, 1983; submitted July 5, 1983; revision received Nov. 7, 1983.

*Senior Engineer.
†LESS Manager.

and heating rates vs flight parameters (angle of attack and Reynolds number).

It should be stressed that the present analysis is directed at establishing and correlating the heating rates experienced during the Orbital Flight Test (OFT) program. The empirical comparison between flight and wind tunnel heating correlation is performed without detailed analysis of the local flowfields at wind tunnel and flight conditions. Flowfield analysis is required to account for changes between wind tunnel and flight conditions in terms of fluid dynamic parameters (i.e., gas chemistry) and surface catalysis.

Thermal Analysis Methodology

Nose Cap and Wing Leading Edge

Comprehensive thermal mathematical models developed and verified with full-scale certification test articles[6] were used to simulate the thermal response of the RCC NC and WLE panels. Since thermocouples could not be reliably installed on the RCC surface because of extreme temperatures, optical radiometers were used to monitor the RCC inner moldline (IML) surface temperature along with thermocouples attached to internal insulation surfaces. Using flight data in conjunction with the multidimensional thermal models, the external outer moldline (OML) temperatures and heating rates were calculated. Internal and cross-radiation effects from the hotter RCC windward surfaces to the cooler leeward area were a significant element of these analyses.

WLE and NC convective heating is calculated using conventional analytical equations for stagnation regions and leading edges.[6] Leading-edge heat flux levels and heating distribution for the highly swept glove section of the wing, the 45 deg swept wing, and the wing tip were derived primarily from subscale model wind tunnel data that were scaled for flight analysis. Existing multidimensional NC three-dimensional (3-D) and WLE two-dimensional (2-D) thermal analysis models, nominal entry heating, and wind tunnel-derived heat flux distributions were used to calculate RCC skin temperatures for the NC and WLE. Revised heating levels were obtained by comparison of predicted and measured STS flight temperatures.

Reusable Surface Insulation

The NONLIN/INVERSE program[2,3] has been used to perform thermal analyses on the instrumented reusable surface insulation (RSI) tiles. These analyses consisted of calculated surface temperature and heating rate and the in-depth thermal response plus an estimation of thermocouple depth, when applicable. The NONLIN/INVERSE program, using embedded thermocouple temperature data, with the use of variable thermal properties (as functions of temperature and pressure) accounts for the effects of radiation loss and interior conduction in computing both surface heating and in-depth thermal response.

Each centerline and wing thermal model, from the OML to the structure, consisted of the HRSI, 0.0075-in. room temperature vulcanizing material RTV-560, 0.160-in. felt, 0.0075-in. RTV-560, and aluminum. The first in-depth thermocouple was used as a boundary condition to drive the thermal model. The initial temperature profile was determined from the temperature of the thermocouples at entry interface. The backwall of the aluminum was assumed to have an adiabatic boundary condition. A one-dimensional inverse transient heat conduction analysis was used to calculate heating rates from in-depth thermocouple measurements.

A typical example of the temperature data in-depth comparisons that have been made for a plug-instrumented tile (wing lower surface 50% semispan, 36% chord) can be seen in Fig. 1. These values were obtained by linear interpolation between nodes from the analysis results. The consistency that has been obtained with this type of comparison for the first five flights indicates that the thermocouple plugs remained fairly stationary from flight to flight and were not excessively jarred from either the buffeting of ascent and entry or by the impact upon landing. For this example (Fig. 1), the effects of the transition from laminar to turbulent flow are not propagated much below the 0.75-in. thermocouple.

An example of the calculated heating rate derived from flight data (lower fuselage, $X/L = 0.50$) can be seen in Fig. 2. In this figure, it can be seen that with the onset of transition the heating rate increased by a factor of 4. The corresponding percent error between the heating rate derived from using the NONLIN/INVERSE program and radiation equilibrium was calculated from the analysis results. For this comparison it was assumed that the NONLIN/INVERSE heating rate is the true solution and the radiation equilibrium heating rate, $\sigma\epsilon T^4$, is the approximation. The largest percent error occurs in three time regimes: the initial heating phase (approximately 60%), during the transition from laminar to turbulent (approximately 25%), and later in the trajectory when the convective heating is essentially zero. During the period of maximum heating, however, the percent error is less than 10%.

Flight Performance

Successful completion of the initial flights of Columbia have provided sufficient data from radiometers, thermocouples, and pressure transducers to appraise the aerothermodynamic/TPS performance. STS flight parameters, especially angle of attack,

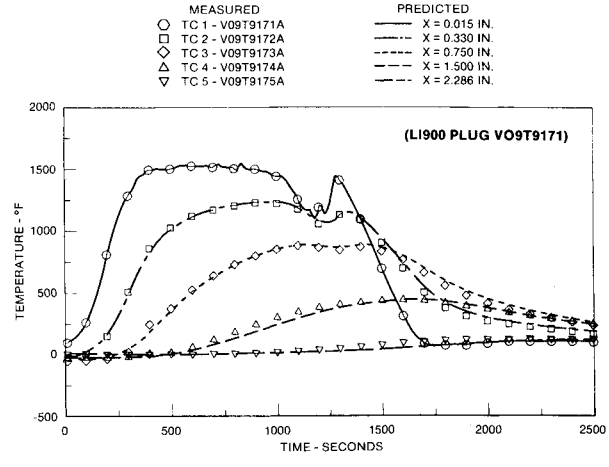

Fig. 1 STS-2 predicted and measured temperature using best estimated thermocouple depth (lower wing 50% semispan, 36% chord).

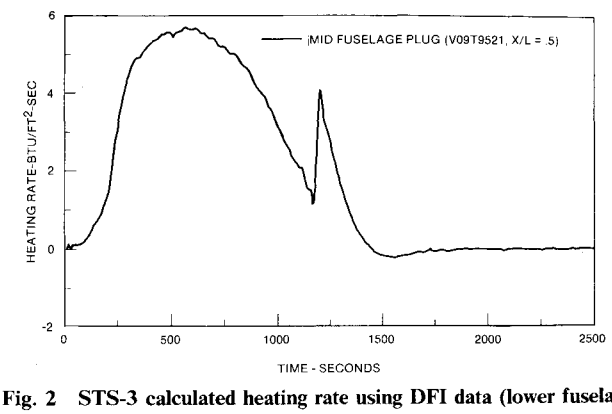

Fig. 2 STS-3 calculated heating rate using DFI data (lower fuselage, $X/L = 0.50$).

allowed relatively lower reference total heat load and heating rates than that predicted for the design trajectory[7] (see Fig. 3).

Over 2,000 development flight instruments (DFI) were installed on the Space Shuttle Columbia to permit the assessment of aerothermal/TPS performance. The majority of the DFI flight data was recorded during ascent and entry. Additional instrumentation (real-time) was used to monitor thermal subsystems continuously during the flight. This analysis, however, is restricted to a few select instruments on the vehicle centerline and wing (see Fig. 4).

Nose Cap

Nose cap radiometer temperature measurements of the IML for the RCC shell were suspiciously low for the first four STS flights. An inspection of the four nose cap radiometers after STS-4 revealed a heavy black deposit on the lenses. The radiometer lenses were cleaned and the calibration checked prior to the STS-5 flight. A comparison of predicted and measured stagnation point IML temperatures is presented in Fig. 5‡. As can be seen, the STS-5 flight data (2605° F) is higher (~ 180° F) than the STS-2 prediction (2425° F) and approximately equal to the predicted design temperature (2575° F) for the 14414.1C design trajectory. By using the nose cap heat flux distribution and the three-dimensional nose cap Thermal Mathematical Systems Simulation Model (TMSSM),[6] analytical heat flux distributions for the postflight STS-2 and 14414.1C design trajectories, respectively, can be illustrated by Figs. 6 and 7. These results indicated that for the STS-5 flight, the nominal peak heating rate prediction was low and the heat flux distribution in error. Use of the design heat flux provides a better temperature comparison, but the heat flux distribution is still not correctly predicted. Since only one set of flight data is available, i.e., STS-5, it is not possible to determine whether these results are typical of the first four flights. However, an assessment of other flight data measurements for the nose cap system, especially interior structural thermal response measurements, indicates that the STS-5 data were similar to previous flight results.[7,8]

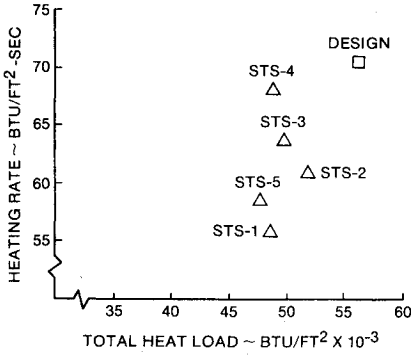

Fig. 3 Comparison of reference heating conditions (design vs STS-1 through STS-5).

Wing Leading Edge

In contrast to the nose cap, radiometer measurements of the wing leading edge IML temperature have been obtained from all STS flights (Fig. 8).§ The maximum heating zone (44% to 55% semispan) results from the interaction of the nose cap bow shock and wing shock which produce higher boundary layer pressures and heat rates. Comparison of predicted and measured RCC shell IML temperatures indicates heat flux levels substantially lower than predicted for Panels 4 and 22, excellent agreement for Panel 16, and heat flux levels higher

‡Subsequent to the preparation of this manuscript recalibration tests on the four NC radiometers indicate the measured STS-5 RCC IML temperatures may have a maximum temperature error of +180°F, i.e., 2605°F may be 2418°F.

§Based on NC radiometer recalibration tests, the WLE flight radiometer temperature measurements are considered suspect. Additional calibration tests are required to determine any temperature variations in the data presented.

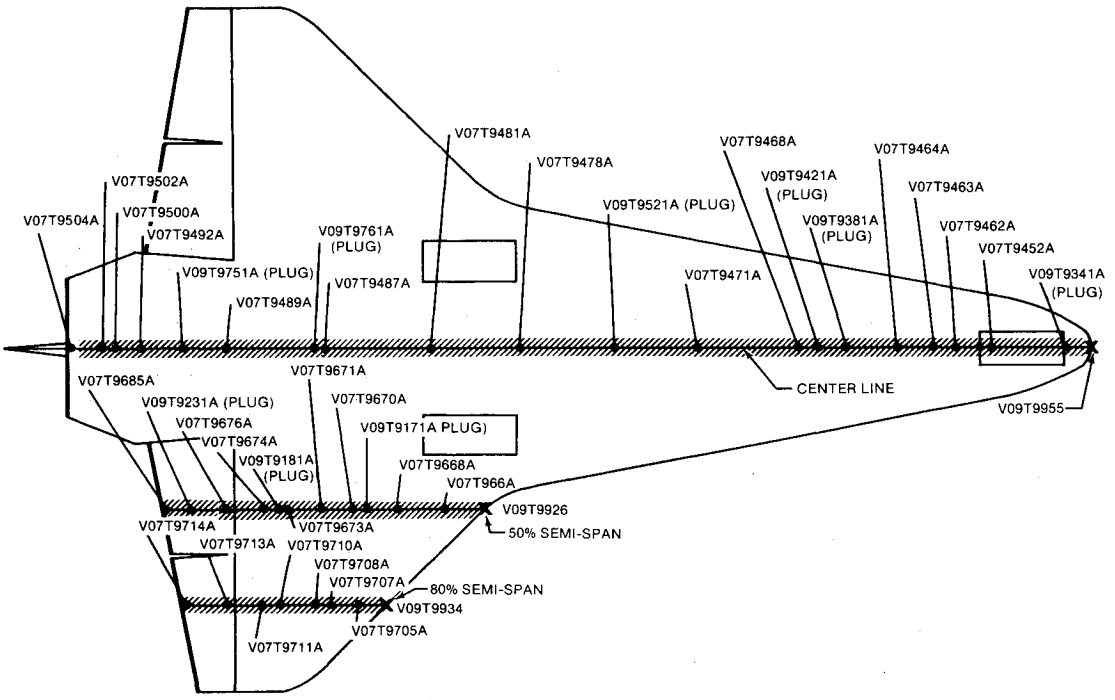

Fig. 4 Location of DFI lower surface instrumentation on Columbia (centerline and wing 50% and 80% semispans).

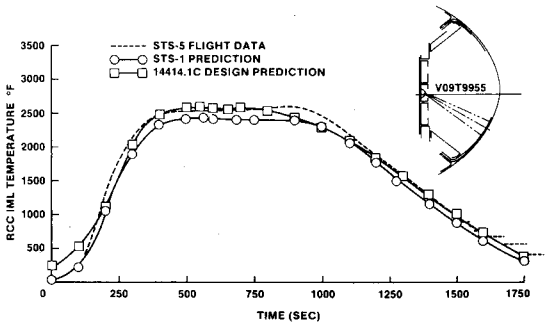

Fig. 5 Nose cap RCC IML temperature.

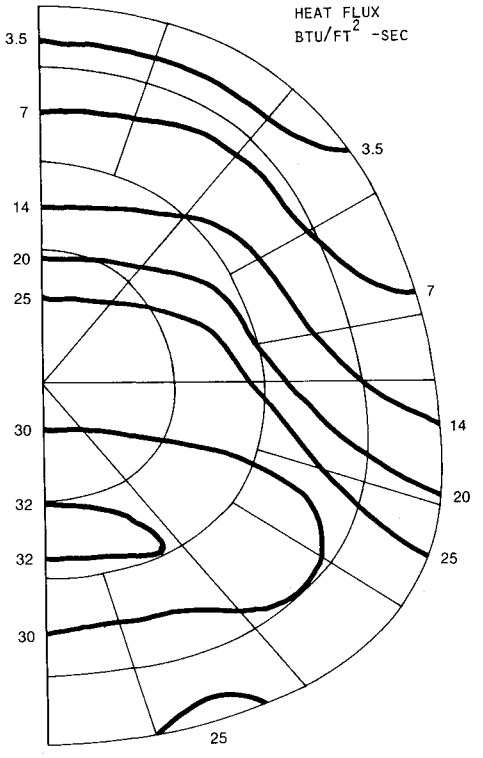

Fig. 6 RCC nose cap STS-2 predicted peak heat flux distribution.

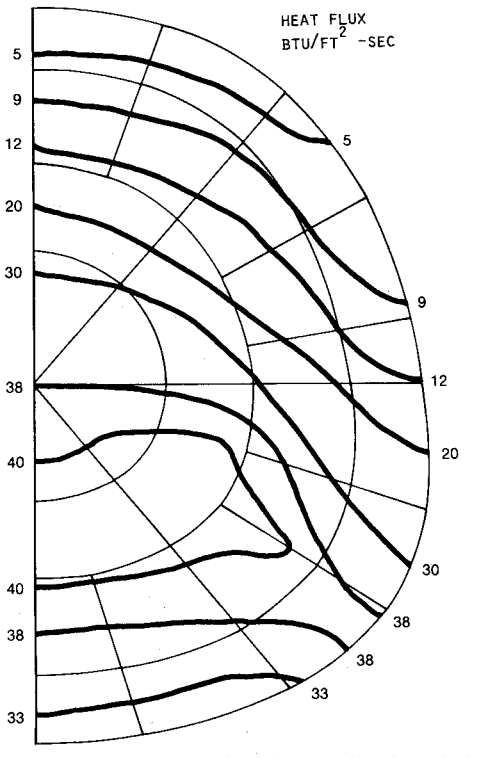

Fig. 7 RCC nose cap 14414.1C design predicted peak heat flux distribution.

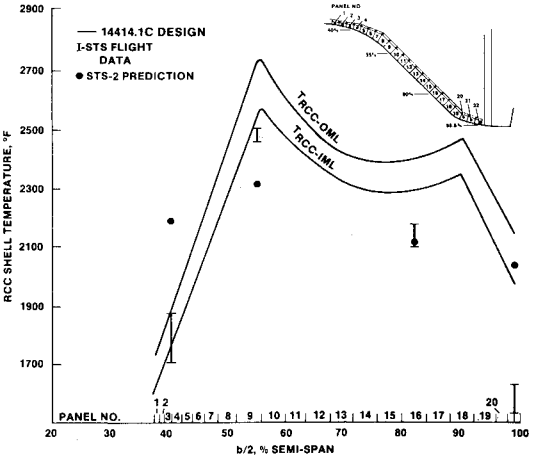

Fig. 8 Wing leading edge (LE) inner moldline temperatures.

than predicted for Panel 9. Wing Panel 9 is located in the "double shock" heating zone, and the results shown in Fig. 9 indicate the measured RCC IML temperature, 2501° F, to be higher (~ 200° F) than the corresponding STS prediction.

Peak heating rate [STS-2 nominal (NOM), STS-2 root sum square (RSS), 14414.1C design] as a function of Panel 9 wetted surface is shown in Fig. 10. Using the wing leading edge two-dimensional TMSSM, the Panel 9 convective heating has been arbitrarily increased to obtain better agreement between measured and predicted temperatures.[8] The Panel 9 analysis indicates that flight correlated heating rates are 25% to 50% higher than predicted for the leeward and windward surfaces. Therefore, the Panel 9 correlated peak heating rate is similar to the predicted 14414.1C nominal design heating.

In contrast to the Panel 9 results, predicted and measured IML temperatures from Panel 16 are in excellent agreement (Fig. 11). The predicted Panel 16 temperature was obtained using the STS-2 nominal heat flux distribution. The overprediction of temperature for both Panel 4 (wing glove) and

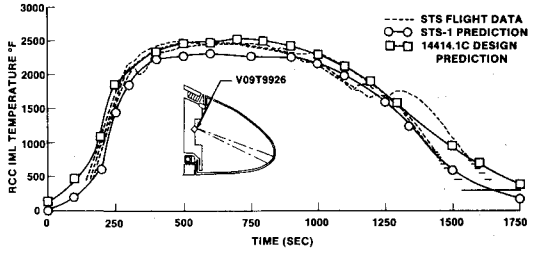

Fig. 9 Wing leading edge (LE) RCC Panel 9 IML temperature.

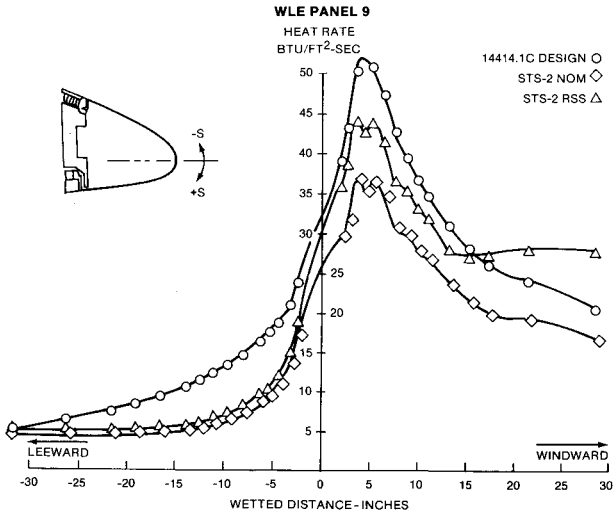

Fig. 10 Heat rate vs wetted distance.

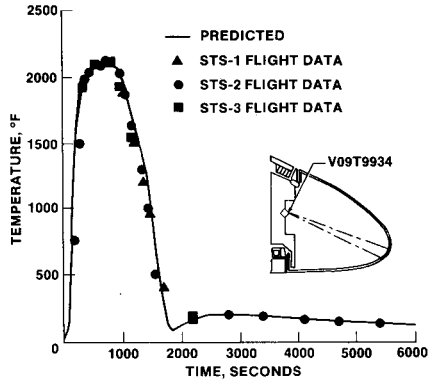

Fig. 11 Panel 16 maximum heating radiometer temperature comparison.

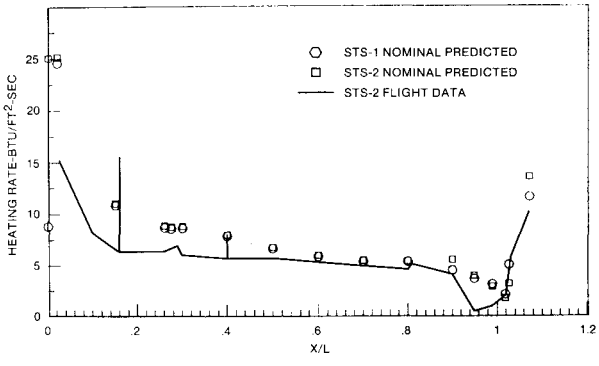

Fig. 12 STS-2 centerline heating distribution compared to STS-1 and STS-2 nominal predicted heating at 600 s.

Panel 22 (wing tip) was not unexpected, since the design heating approach (i.e., swept cylinder) is conservative in regions of high sweep.

Fuselage Lower Surface—Centerline Analysis

The lower surface TPS consists of the RCC NC and RSI tiles on the fuselage and body flap (BF) (see Fig. 4). The NC temperature/heating environment is based on predictions using data from radiometers installed in the NC cavity and thermocouples on the internal insulation. In contrast to the NC, surface thermocouples were installed under the RSI tile coating and could be used directly (via NONLIN/INVERSE) to obtain heating rates and thermal response characteristics. Along the centerline six tiles were "plug" instrumented (thermocouples installed in depth) which permitted the in-depth thermal response to be monitored and analyzed in a manner similar to that shown in Fig. 1.

A typical heating rate response distribution for STS-2 flight data compared to STS-1 and STS-2 preflight predictions[4] at 600 s can be seen in Fig. 12. The heating rate discontinuities at $X/L = 0.16$ and 0.40 are due to two catalytically coated tiles. The greatest disagreement between flight and predicted data is forward of the $X/L = 0.6$ station. As can be seen in Fig. 12, the flight data (via NONLIN/INVERSE) is consistently lower than the preflight predictions.

Of more interest is the comparison of the heating rate distribution for STS-2, STS-3, and STS-5 flight data at a freestream Reynolds number of 1×10^6. The Mach number and angle of attack at this Reynolds number are essentially the same for all three flights. As can be seen in Fig. 13, the heating rate distributions for STS-2 and STS-3 are essentially identical. The heating rate distribution for STS-5 is approximately 13% greater than either STS-2 or STS-3 at $X/L = 0.026$. From $X/L = 0.6$ to $X/L = 1.0$ the heating rate distribution is essentially the same for all three flights. The heating rate distribution for STS-5 is above the STS-2 and STS-3 heating data forward of $X/L = 0.6$. This increase could be explained if the reference (1 ft sphere) heating for STS-5 is greater than that for STS-2 or STS-3. However, when a comparison of the reference heating rates is made, STS-2 is 1.3% lower than STS-3, and the reference heating for STS-5 is 6.8% lower than STS-3 for the 1×10^6 Reynolds number condition. This comparison implies exactly the opposite effect on the STS-5 heating rate distribution from that shown in Fig. 13. The results shown in Fig. 13 are similar to those obtained at other Reynolds numbers (with corresponding consistent Mach numbers and angles of attack).

If the STS-5 Best Estimated Trajectory (BET) was in error by 15% to 20% (pressure and density too low), the increase in heating could be explained without considering surface properties change. MINIVER,[9] using BET data, was used to predict the local pressure along the centerline for STS-2, STS-3, and STS-5. These deduced pressures were then compared to flight data at corresponding X/L locations. The percent variation between the predicted and measured pressures was consistent between each flight. These comparisons tend to validate the accuracy of the BET data.

Some of the increase in heating for STS-5 could be attributed to tile slumping by the tile adjacent to V09T9341A ($X/L = 0.026$) and to the greater number of catalytic tiles along the centerline. However, the effects of catalycity appear to have only a local effect on heating as can be seen in the STS-2–STS-3 comparison. Indeed, this local effect should also be true for V09T9341A since the behavior of the adjacent slumped tile should have a minimal influence on the heating for V09T9341A.

This set of comparisons indicates that the lower surface tiles had a change in surface properties after STS-3. In examining the heating rate distribution in Fig. 13, the surface degradation effect is greatest for those tiles which experienced heating rates in excess of 5 Btu/ft^2-s at $Re_\infty = 1 \times 10^6$ with a more pronounced effect at higher heating rates.

Wing Surface Analysis

The wing lower surface TPS consists of RCC WLE and RSI tiles. In contrast to the NC, DFI radiometer measurements on the WLE IML temperatures have provided accurate data for comparison of predicted and measured entry temperatures/heating rates. Of particular interest were the 50% and

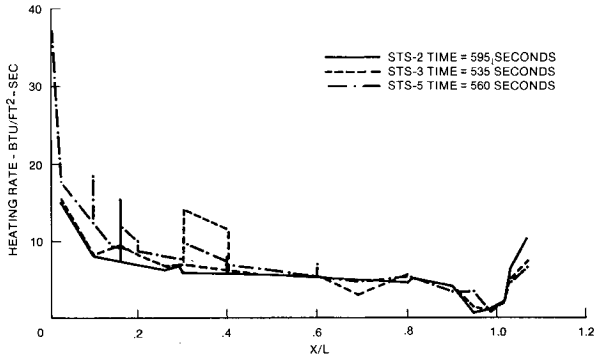

Fig. 13 Comparison of centerline heating distribution for STS-2, STS-3, and STS-5 at $Re_\infty = 1 \times 10^6$.

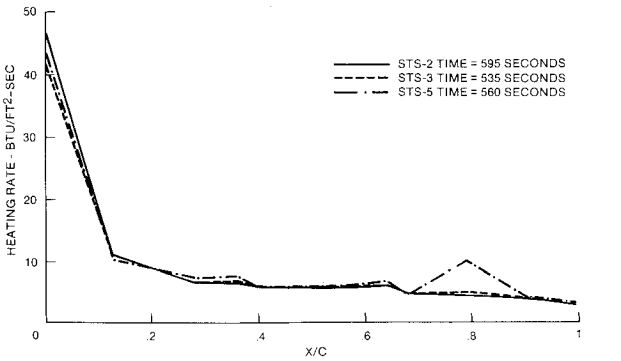

Fig. 14 Comparison of wing 50% semispan heating distribution of STS-2, STS-3, and STS-5 at $Re_\infty = 1 \times 10^6$.

80% semispans (see Fig. 4), since these areas had WLE instrumentation.

There were three plugs on the 50% semispan which permitted the in-depth thermal response to be monitored and analyzed (see Fig. 1). Typical plots of the heating rate chordwise distribution at a freestream Reynolds number of 1×10^6 can be seen in Figs. 14 and 15 for the 50% and 80% semispans, respectively.

It is interesting to observe that the same heating rate characteristics are observed for the 50% wing span as for the centerline, namely, that the heating rate distributions for STS-2 and STS-3 are similar in magnitude, but STS-5 indicates that a hotter environment was experienced for those conditions where the heating rate was greater than 5 Btu/ft^2-s. For STS-5 the large heating indicated at $X/C = 0.79$ may be attributed to the 5 deg elevon deflection, but this does not explain the reduced heating at the elevon trailing edge. In addition, wind tunnel data do not indicate flow separation in this region. It is suspected that the data for $X/C = 0.79$ station are in error.

This increase in heating for STS-5 on the 50% span is further evidence of tile surface degradation after STS-3. In addition, there were no tile slumps or catalytic tiles to influence the upstream flow for this span.

For the 80% span an adequate comparison between STS-2 and STS-3 cannot be made due to instrument malfunction for the first three instruments on STS-3. However, in comparing the results between STS-2 and STS-5, the same increase in heating is observed.

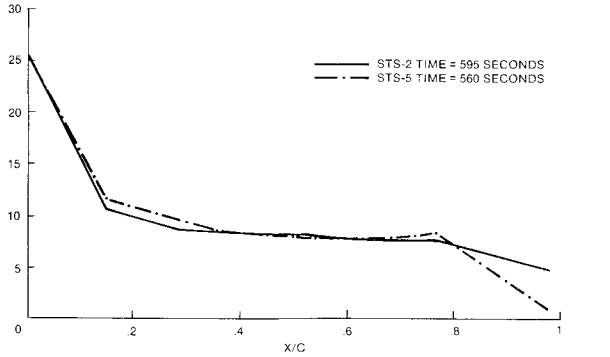

Fig. 15 Comparison of wing 80% semispan heating distribution of STS-2 and STS-5 at $Re_\infty = 1 \times 10^6$.

Flight Data Correlation

The assessment of the TPS environment would not be complete without relating the heating rates derived from the thermal analysis to the flight parameters, such as angle of attack, Mach number, and Reynolds number. The flight data trajectory parameters are obtained from the Johnson Space Center (JSC)/MPAD BET tape for angle of attack, freestream velocity, temperature, and pressure. The corresponding Mach number and freestream Reynolds number are calculated in the standard manner. The reference heating rate to a 1 ft sphere, reference film coefficient, total enthalpy, and normal shock Reynolds number are obtained through the use of the MINIVER program.[9] This program uses correlations of two-dimensional flowfield models normalized to either three-dimensional flowfield computations or empirical results to determine boundary-layer edge properties and heating rates.

Two locations, $X/L = 0.026$ and $X/L = 0.50$, were selected to compare flight data with wind tunnel data. The wind tunnel data (0.9 H_T, recovery enthalpy) were taken at Mach 8.[10] For these two locations the wind tunnel heat rates (h/h_{ref}) indicate a low influence of angle of attack vs Reynolds number. At the higher Reynolds number, low angle of attack that occurred late in flight wind tunnel data is not available. The most significant parameter that can be used in comparing flight data with wind tunnel data is Reynolds number. In these comparison plots, the W.T. data are shown by the appropriate symbol for each angle of attack and the flight data are shown as a solid continuous line. In addition, as an aid in analysis, the corresponding angle of attack (latest time in flight occurrence) is identified for the flight data.

The thermal analysis used flight temperature data to obtain the heating rates. The objective of this analysis is to compare the flight data with wind tunnel data at the same Reynolds number. It was recommended that the normal shock Reynolds number[11] can adequately be used to correlate wind tunnel data with flight data. The advantage of using normal shock Reynolds number (Re_{NS}), as compared to freestream Reynolds number (Re_∞), is that the Re_{NS}, to a first order, accounts for the real gas effects. The scaling parameter (Re_{NS}/Re_∞), determined from the test environment (at Mach 8), for the wind tunnel data is 0.1121.

The comparison of wind tunnel data and flight data for V09T9341A ($X/L = 0.026$) for STS-3 and STS-5 can be seen in Figs. 16a and 16b. Data for STS-2 can be seen in Ref. 12. The W.T. data shown in these figures were obtained by linear interpolation of data from the $X/L = 0.02$ and $X/L = 0.03$ locations.

The analysis results derived from this instrument are of interest since this tile experienced the highest level of heating for any instrumented tile on the fuselage. Considering the significant differences between wind tunnel and flight local flow conditions, enthalpy level, and air properties, the correspondence between flight data and wind tunnel data is quite

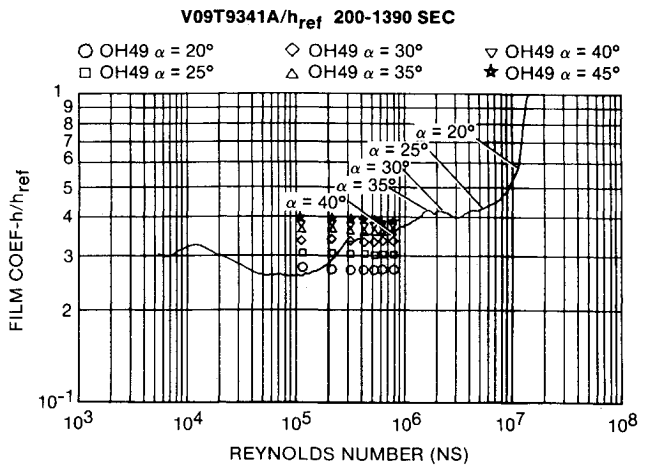

Fig. 16a Comparison of STS-3 heating with wind tunnel data vs Re_{NS} for V09T9341A (centerline, $X/L = 0.026$).

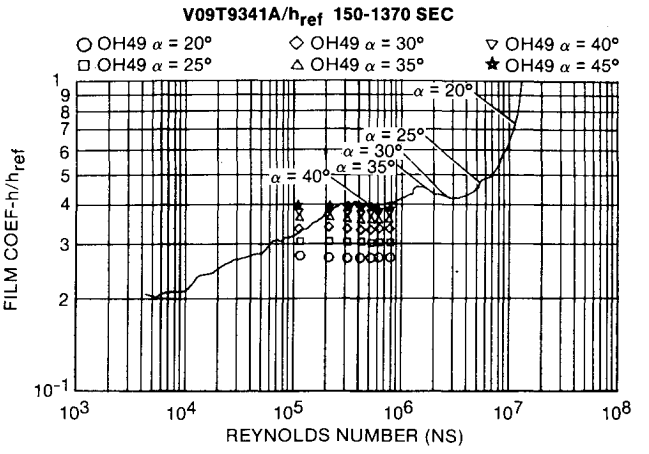

Fig. 16b Comparison of STS-5 heating with wind tunnel data vs Re_{NS} for V09T9341A (centerline, $X/L = 0.026$).

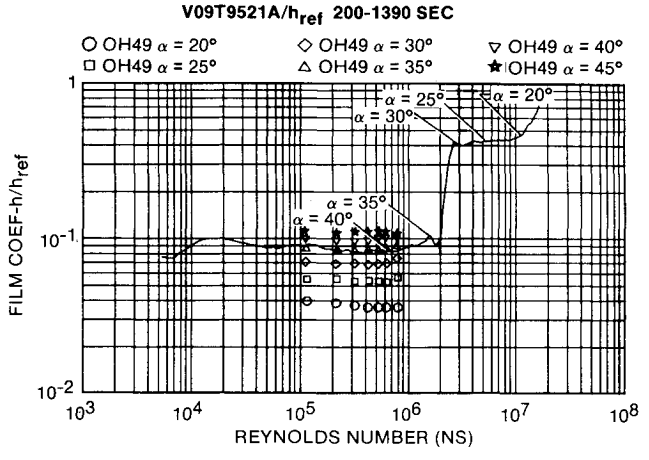

Fig. 17a Comparison of STS-3 heating with wind tunnel data vs Re_{NS} for V09T9521A (centerline, $X/L = 0.50$).

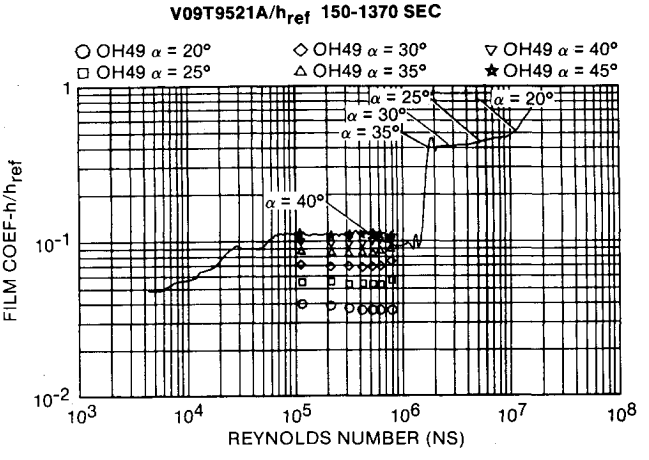

Fig. 17b Comparison of STS-5 heating with wind tunnel data vs Re_{NS} for V09T9521A (centerline, $X/L = 0.50$).

good. The heating rates for STS-2 and STS-3 are essentially the same for all values of Re_{NS}, whereas the heating rates for STS-5 are higher than STS-2 and STS-3.

The comparison of wind tunnel data with flight data for V09T9521A ($X/L = 0.50$) for STS-3 and STS-5 can be seen in Figs. 17a and 17b. Data for STS-2 can be seen in Ref. 13. No interpolation of the W.T. data was required for this semispan. The STS-2 data tend to run between the 35 and 45 deg angle of attack W.T. data, the STS-3 data tend to run through the 35 deg angle of attack W.T. data, and STS-5 data tend to run through the 45 deg angle of attack W.T. data when all three trajectories were flying at essentially 40 deg angle of attack. At high Reynolds number, after transition, all three flights are in agreement. It is interesting to observe, however, that for STS-2 and STS-3, transition occurred below $\alpha = 35$ deg, but for STS-5, transition occurred above $\alpha = 35$ deg. As with V09T9431A, the thermophysical properties (density, specific heat, and thermal conductivity) remained invariant from flight to flight.

This comparison reinforces the observation that was apparent from the X/L heating rate distribution plots, namely that the surface properties for the lower surface changed from STS-3 to STS-5 during early laminar heating. The independent thermal analysis performed with the NONLIN/INVERSE program, however, indicates that the other thermophysical properties (density, specific heat, and thermal conductivity) remained invariant from STS-1 through STS-5.

Early in the STS-4 mission, after analyzing ascent data there was an indication that moisture had penetrated some of the lower surface tiles. This was verified by analyzing Orbiter thermal response data. This water penetration (and subsequent ice formation in the tiles) required the vehicle orientation to be changed (from the original mission plan) to recondition the tiles (i.e., drive the moisture out). In order to prevent interference with STS-5 mission requirements, the Orbiter's lower surface was treated to provide additional waterproofing. Analysis of STS-5 ascent and orbital thermal response indicated that the waterproofing was effective in preventing moisture penetration. It is possible that the increase in heating observed for the forward stations on STS-5 may be due to the waterproofing effects on the surface characteristics. However, from the observed agreement in heating between flights late in time (higher values of Re_{NS}), it is possible that post-STS-5 testing will reveal no significant changes in the lower surface characteristics for the tiles.

Conclusions

A thermal analysis has been performed on the Shuttle Orbiter to determine TPS response characteristics using flight data. Comparisons of preflight predictions with flight data and

flight-to-flight comparisons have been presented along the lower fuselage centerline, lower wing 50% semispan, and lower wing 80% semispan.

Stagnation and peak temperature/heating characteristics for the RCC nose cap and WLE 50% and 80% semispans were analyzed. The results of this analysis indicate higher than predicted heating on the nose cap and 50% semispan WLE panel.

Lower than predicted heating (using STS flight data) was observed on the Orbiter lower windward fuselage centerline, lower wing 50% semispan, and lower wing 80% semispan.

Comparisons of successive flight data using X/L and X/C heating rate distributions were made. The results of this analysis indicated the laminar heating for STS-5 was higher than expected for its trajectory. However, using h/h_{ref} vs normal shock Reynolds number comparisons, agreement between successive flights was obtained at higher Reynolds numbers.

Using flight parameters (h/h_{ref}, Mach number, normal shock Reynolds number, and angle of attack), the wind tunnel data provide a reasonable simulation of environments experienced in flight. The flight heating data obtained on Columbia along with wind tunnel data provide a basis for extrapolation of the heating to other flight conditions.

References

[1]Williams, S.D. and Curry, D.M., "Parameter Optimization—An Aid to Thermal Protection Design," *Journal of Spacecraft and Rockets*, Vol. 9, Jan. 1972, pp. 33-38.

[2]Curry, D.M. and Williams, S.D., "Nonlinear Least Squares—An Aid to Thermal Property Determination," *AIAA Journal*, Vol. 2, May 1973, pp. 670-674.

[3]Williams, S.D. and Curry, D.M., "An Analytical and Experimental Study Using a Single Embedded Thermocouple," *Journal of Spacecraft and Rockets*, Vol. 14, Oct. 1977, pp. 632-637.

vironment of the Space Shuttle Orbiter," AIAA Paper 82-0821, *AIAA/ASME 3rd Joint Thermophysics, Fluids, Plasma, and Heat Transfer Conference*, June 7-11, 1982.

[5]"NASA Langley Conference, Shuttle Performance—Lessons Learned," NASA CP to be published, March 8-10, 1983.

[6]Curry, D.M., Cunningham, J.A., and Frahm, J.R., "Space Shuttle Orbiter—Leading Edge Structural Subsystem Thermal Performance," AIAA Paper 82-004, *AIAA 20th Aerospace Sciences Meeting*, Jan. 11-14, 1982.

[7]Dotts, R.J., Smith, J.A., and Tillian, D.J., "Space Shuttle Orbiter Reusable Surface Insulation Flight Results," presented at NASA Langley Conference on Shuttle Performance: Lessons Learned, March 8-10, 1983.

[8]Curry, D.M., Latchem, J.W., and Whisenhunt, G.B., "Space Shuttle Orbiter Leading Edge Structural Subsystem Development," AIAA Paper 83-0483, *AIAA 21st Aerospace Sciences Meeting*, Jan. 11-13, 1983.

[9]Hender, D.R., "A Miniature Version of the JA70 Aerodynamic Heating Computer Program, H800 (MINIVER)," Ret. MDC G0462, McDonnell Douglas Astronautics Company, Huntington Beach, Calif., June 1970, revised Jan. 1972.

[10]Martindale, W.R., Kaul, C.E., and Nutt, K.W., "Test Results from the NASA/Rockwell International Space Shuttle Orbiter Heating Test (OH49B) conducted in the AEDC-VKF Tunnel B," Ret. AEDC-DR-74-73, VonKarman Gas Dynamics Facility, ARO, Inc., Arnold Engineering Development Center, Arnold Air Force Station, Tenn., Sept. 5, 1974.

[11]Ried, R.C., Jr., Goodrich, W.D., Strouhal, G., and Curry, D.M., "The Importance of Boundary Layer Transition to the Space Shuttle Design," *Proceedings of the Boundary Layer Transition Workshop*, Nov. 3-5, 1971, Aerospace Report No. TOR-0172 (S2816-16), Dec. 1971.

[12]Williams, S.D., "Columbia: The First Five Flights Entry Heating Data Series, Volume 3, The Lower Windward Surface Centerline," NASA CR-171665, May 1983.

[13]Williams, S.D., "Columbia: The First Five Flights Entry Heating Data Series, Volume 4, The Lower Windward Wing 50% and 80% Semi-Spans," NASA CR-171666, May 1983.